Frau Prof. Dr. Emilie Jäger gewidmet

Excess Ar geochemistry in potassic volcanites

by *Igor M. Villa*[1]

Abstract

$^{40}Ar/^{39}Ar$ age spectra of leucites, sanidines and a kalsilite from the Quaternary Roman Volcanic Province (central Italy) frequently feature excess ^{40}Ar released only at high temperature. In leucites from the Alban Hills, Ar isotopic compositions can be very radiogenic (blank-corrected $^{40}Ar/^{36}Ar$ ratios over 6,000); in sanidines from Vulture, the excess is shared by total rock sanidines and pumice sanidines, but is partly removed by leaching. An orthoclase megacryst from Mt. Erebus, Antarctica, also displays a large Ar excess, but only at low temperatures.

Multi-element correlation plots are used to investigate possible correlations of excess Ar with anion sites (represented by chlorine-derived ^{38}Ar) and with Ca-bearing exsolutions. Neither exists.

Individual fluid inclusions in a hydrothermal anhydrite from the Roman Volcanic Province were analyzed with a laser microprobe. Excess ^{40}Ar ($^{40}Ar_{xs}$) was present, but the exact isotopic composition is ill constrained, owing to counting rates below 100 ions/sec.

The high-temperature $^{40}Ar_{xs}$ is a primary characteristic of the minerals and was indigenous to the magmas; in the present case it cannot derive from partly degassed restitic material and cannot be carried by fluid inclusions. It must be sought in a process operating at sufficient depth to affect sanidines already formed in pumices without analcimizing the leucites. The fluid carrying the ^{40}Ar anomaly was either surface water having leached old continental crust or, more probably in this case, a magmatic, water-poor fluid which derives its Ar from the mantle.

Keywords: $^{40}Ar/^{39}Ar$ dating, Ar excess, Ar geochemistry, crystal lattice sites, Roman Volcanic Province.

1. Indroduction

The occurrence of excess ^{40}Ar (hereafter $^{40}Ar_{xs}$) has bothered geochronologists working on metamorphic and plutonic rocks (e.g. BREWER, 1969; FOLAND, 1983) but little systematic effort has been devoted to assessing its presence in volcanic rocks. Since the early days of DALRYMPLE's (1969) observation of excess Ar in five basalts, geochronologists' reports on $^{40}Ar_{xs}$ in volcanites have been surprisingly rare, despite the geochemists' reports of very large ^{40}Ar enrichments in magmatic gases. One difficulty is that unless $^{40}Ar/^{39}Ar$ is used, the only criterion to diagnose $^{40}Ar_{xs}$ is the discordance of stratigraphy and K/Ar dates; however, causes other than bona fide $^{40}Ar_{xs}$ may have brought about this discordance (e.g. analytical problems), and this may explain why published work usually does not include stratigraphically discordant samples. On the contrary, $^{40}Ar_{xs}$ must no longer be considered a nuisance and hidden away in shame; rather the collective effort should be aimed at understanding the wherefore and why of its distribution.

The present work addresses the geochemistry of excess Ar by studying its distribution in magmatic minerals, attempting to eliminate the effects both of xenocryst contamination and of groundmass alteration, which could potentially perturb whole rock samples. $^{40}Ar/^{39}Ar$ experiments were performed on leucites, kalsilite and sanidines, mostly from the Roman Volcanic Province (RVP) in Central Italy. RVP volcanites consist of silica-undersaturated, K-rich ignimbrites and lavas (WASHINGTON, 1906). The stratigraphies of all volcanic centres are well studied.

[1] Istituto di Geocronologia CNR, Via Maffi 36, I-56127 Pisa.
Present address: Abt. für Isotopengeologie der Universität Bern, Erlachstr. 9a, CH-3012 Bern.

The only non-Italian sample in this work is a 10 cm orthoclase megacryst from the 1983 eruption of Mt. Erebus, Antarctica.

The isotopic compositions of Ar in individual fluid inclusions of a hydrothermal anhydrite from a geothermal field in the RVP were analyzed with a laser microprobe. The reason for this investigation was trying to understand if all fluid inclusions in an area of the RVP presumably underlain by hot magma represent one and the same fluid, or if two components are being mixed, i.e. a shallow and a magmatic fluid, under the assumption that their isotopic signatures be different.

2. Analytical techniques

Minerals were separated using standard magnetic methods and heavy liquids; handpicking was used only for VU 1813-P. The Erebus orthoclase megacryst ($10 \times 2 \times 1.5$ cm) was scraped free of the adhering black glass with a steel chisel, then a 1 mm slice was sawed and analyzed as a chunk, without further treatment. No attempt was made, purposefully, to eliminate the zillions of dark inclusions it contained. During the stepwise heating, the slice started crumbling around 1000°C and had fallen apart into mm-sized pieces at 1200°C, but the gas release only ceased at 1600°C.

Neutron irradiations were performed at the TRIGA reactor, University of Pavia; neutron doses for the various irradiation packages were a few times 10^{16} n/cm^2. The SH2 anhydrite for the laser experiment received 7×10^{15} n/cm^2 in the Herald reactor, Aldermaston. Monitor minerals were muscovite B4M (FLISCH, 1982) and intralaboratory standard leucite VS-3 (RADICATI et al., 1981), recalculated with FLISCH's (1982) value for B4M. The VS-3 analyses were performed on single, cm-sized crystals. Interference corrections were: $(^{39}\text{Ar}/^{37}\text{Ar})_{\text{Ca}} = .00067$; $(^{38}\text{Ar}/^{37}\text{Ar})_{\text{Ca}} = .00023$; $(^{36}\text{Ar}/^{37}\text{Ar})_{\text{Ca}} = .00027$; $(^{40}\text{Ar}/^{39}\text{Ar})_{\text{K}} = .008$; $(^{38}\text{Ar}/^{39}\text{Ar})_{\text{K}} = .01$.

A synthetic 0-age standard, SOS (VILLA, 1987) was also used to make sure no artefact affected the data.

Ar was extracted in 25 minute steps by RF heating of a machined Mo crucible in 25 minute steps and purified in an all-pyrex system comprising a hot Ti sponge and two SAES Zr-Al getters. The temperature control on the RF furnace was indirect via the grid current reading, so that absolute temperature are probably no more accurate than 5%. Blank amounts were $2–3 \times 10^{-9}$ ml atmospheric Ar below 1100 °C rising to 2×10^{-8} ml at 1700 °C. For the leucites, the sample-derived ^{36}Ar was much smaller than the blank ^{36}Ar and

this created large uncertainties on the trapped Ar in calculating isochron plots (not on ages, though, as blanks were atmospheric).

Data for unpublished samples are presented in table 1 after machine corrections (background and 0.95%/amu mass discrimination) and ^{37}Ar decay.

Hydrocarbons, of possibly primary origin, were sometimes found in volcanic rocks in earlier work, so that a specially high activation voltage (30 V) on the SAES getters was used to eliminate them from steps below 600–700°C (at higher temperature, hydrocarbons are gradually running out, and the Mo crucible starts to act as a getter itself); their presence would create an artificially low age by producing excesses at masses 36 and 39. Their absence from the present samples was monitored by measuring peaks at masses 41 to 43.

The MAT 240 all-metal mass spectrometer is equipped with a Baur-Signer source and a double collector (Faraday cup + electron multiplier). Ar concentrations were determined by extrapolating peak heights to the inlet time. Corrections were made for machine background and mass discrimination, but (in most cases) not for Ca-produced interferences since ^{37}Ar had decayed prior to measurement. However, this correction is negligible in sanidines and leucites.

Fluid inclusion data were obtained with the laser microprobe of the Physics Department, Sheffield University. A Nd-glass pulsed laser was focussed through a microscope onto the sample contained in a high-vacuum chamber connected to a mass spectrometer. The focussed beam has a diameter of 25 μm with a power density of 10^7 W/cm^2. The permanent spectrometer background was about 10^{-14} ml for masses 36 and 38; it was monitored very frequently (about twice each shot) and found to be reproducible to about 20%.

3. $^{40}\text{Ar}/^{39}\text{Ar}$ data

3.1. Ar$_{xs}$ IN LEUCITES

The first discussion on leucite spectra demonstrating the presence of Ar$_{xs}$ was presented by VILLA (1985a). The leucites of that study came from the Alban Hills, whose lavas and ignimbrites all contain leucite. The history of the Alban Hills volcano can be crudely summarized as follows (BERNARDI et al., 1982; VILLA, 1991; FUNICIELLO and VILLA, unpublished data): 0.48 Ma bp, onset of activity with stratocone lavas and ignimbrites; 0.35 Ma bp, Villa Senni tuff eruption and caldera formation; stasis until 0.27 Ma bp, followed by brief lava episodes. The chemical uniformity and
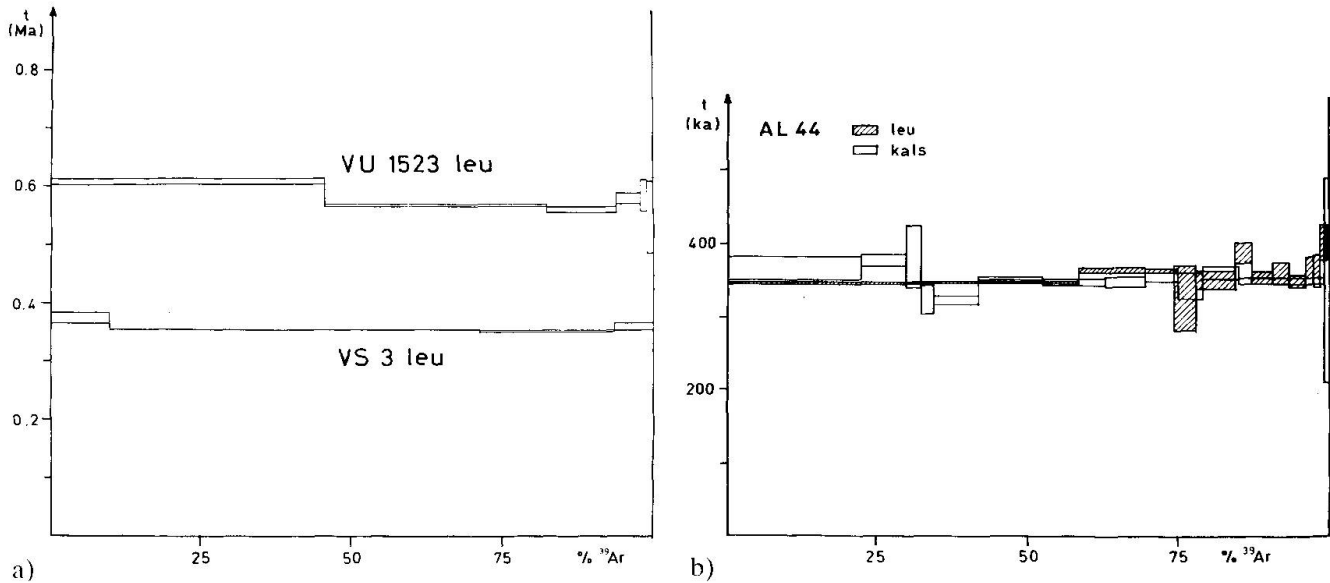
Fig. 1 Flat ^{40}Ar/^{39}Ar age spectra of (a) coarse-grained leucites VS3 and VU 1523; (b) coexisting coarse-grained leucite and kalsilite AL 44.

the good chronostratigraphic framework make the Alban Hills a perfect case history to investigate excess Ar in leucites.

The leucites from the Alban Hills fall in two very different varieties. The "large" ones are cm-sized, euhedral phenocrysts from evolved tuffs; the "small" ones derive from primitive, aphyric lavas whose natural grain size is around 100 μm. Age spectra of the "large" leucites are flat. Three examples of "large" Alban Hills leucites are shown in figures 1a–b. VS–3, from the Villa Senni marker tuff, was dated by RADICATI et al. (1981) and used in Pisa as intralaboratory standard. One typical spectrum of the dozen that were obtained is shown in figure 1a, together with leucite VU 1523 (see § 3.2). Another example from the Alban Hills, AL-44, is from a decimeter-sized xenolith with a very unusual kalsilitoitic composition, brought to surface by the Villa Senni eruption (FEDERICO, 1976; BELKIN et al., 1991): coexisting leucite and kalsilite crystals are typically 2–3 mm large. Both are shown in figure 1b.

Quite on the contrary, step ages of the "small" leucites become constantly higher (Fig. 2), up to several Ma (the highest step age is 299 ± 2 Ma in AL-42); this ^{40}Ar$_{xs}$ component is released at temperatures above 800–900°C, when over 95% of the ^{39}Ar is degassed (Fig. 3 a, b). In at least one case, a little Ar was released in the step after the leucite had visibly melted. This behaviour may be due to the very high viscosity of the leucitic liquid (RAMMENSE, pers. comm.) which may not convect all of the gas to the surface in the 25 minutes of the melting step. These results can be displayed in a differential release plot (Fig. 3 a, b) which shows

a single release peak for ^{39}Ar and a characteristic double-humped "Camel" pattern for ^{40}Ar. That is to say, in the low-temperature release ^{40}Ar and ^{39}Ar$_K$ are related to each other, but in the well-distinct high-temperature hump the ^{40}Ar is "parentless", i.e. unsupported by ^{39}Ar$_K$.

Another way to visualize the same results is on a ^{36}Ar/^{40}Ar vs ^{39}Ar/^{40}Ar three-isotope plot. In this modified isochron, age is the inverse of the abscissa intercept, trapped Ar is the ordinate inter-
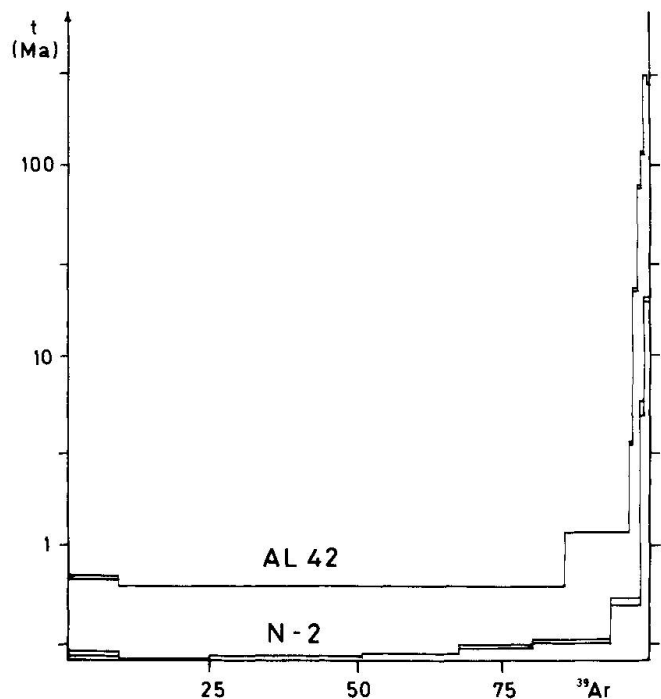

Fig. 2 Age spectra of fine-grained leucites N-2 (data in VILLA, 1991) and AL 42. Note log scale.

Tab. 1 Stepwise heating data. All isotopes are in pl/g and were corrected only for spectrometer background and discrimination and for ^{37}Ar decay, where applicable. The J-value was determined by Ni-counting and comparison with monitor minerals. Only for monitor VS3 was it calculated assuming t = 351 ka.

AL 42   0.204g   J = .00036

step	T	^{40}Ar$_{tot}$	^{39}Ar	^{36}Ar	t ± 1 σ
1	400	77.2 ± .5	31.33 ± 4	.152 ± 1	0.668 ± .10
2	500	297.3 ± .55	276.72 ± .55	.147 ± 1	0.596 ± 2
3	570	132.0 ± .2	41.21 ± 5	.191 ± 1	1.190 ± 5
4	640	32.3 ± .2	3.07 ± 1	.053 ± 1	3.509 ± 46
5	700	96.1 ± .3	2.19 ± 1	.068 ± 1	22.58 ± 1
6	800	152.8 ± .3	1.11 ± 1	.066 ± 1	76.26 ± .41
7	1000	335.3 ± .3	1.63 ± 1	.104 ± 1	117.5 ± .6
8	1200	710.9 ± .8	1.33 ± 1	.150 ± 1	300.0 ± 1.7
9	1600	435.8 ± .4	0.70 ± 1	.384 ± 2	276.2 ± 2.4

AL 44 - lc   0.2146g   J = .000118

step	T	^{40}Ar$_{tot}$	^{39}Ar	^{36}Ar	t ± 1 σ
1	400	282.0 ± .6	71.521 ± .129	.5600 ± 22	0.347 ± 2
2	500	86.4 ± .2	19.345 ± 72	.1805 ± 13	0.364 ± 4
3	600	29.5 ± .2	4.460 ± 28	.0768 ± 27	0.323 ± 44
4	700	89.0 ± .1	7.758 ± 10	.2583 ± 14	0.349 ± 12
5	800	34.1 ± .1	3.195 ± 7	.0960 ± 7	0.387 ± 14
6	900	25.9 ± .2	4.331 ± 7	.0635 ± 5	0.351 ± 8
7	1000	23.2 ± .2	3.544 ± 7	.0583 ± 1	0.357 ± 16
8	1100	18.2 ± .1	3.117 ± 5	.0444 ± 4	0.346 ± 9
9	1150	11.9 ± .1	1.653 ± 4	.0307 ± 4	0.366 ± ,15
10	1200	12.1 ± .1	1.043 ± 3	.0333 ± 4	0.36⊦ ± 22
11	1600	50.2 ± .1	2.175 ± 3	.1559 ± 12	0.406 ± 33

VU 1523   0.075g   J = .0001142

step	T	^{40}Ar$_{tot}$	^{39}Ar	^{36}Ar	t ± 1 σ
1	550	469.8 ± 1.3	60.282 ± .206	.9887 ± 48	0.6070 ± 55
2	600	228.0 ± .2	49.259 ± 81	.3136 ± 114	0.5659 ± 20
3	700	94.2 ± .2	15.092 ± 17	.1801 ± 11	0.5594 ± 46
4	800	71.2 ± .1	5.402 ± 6	.1894 ± 9	0.5804 ± 106
5	950	75.8 ± .1	1.970 ± 6	.2373 ± 9	0.5856 ± 275
6	1600	34.4 ± .1	0.566 ± 3	.1113 ± 6	0.5501 ± 623

AL 44 - ks   0.1154g   J = .000122

step	T	^{40}Ar$_{tot}$	^{39}Ar	^{36}Ar	t ± 1 σ
1	400	226.5 ± 3.2	35.79 ± 7	.565 ± 9	0.365 ± 17
2	500	59.2 ± .3	11.63 ± 1	.133 ± 1	0.377 ± 8
3	600	35.2 ± .3	3.79 ± 1	.097 ± 3	0.381 ± 47
4	700	20.6 ± .1	3.24 ± 1	.054 ± 1	0.322 ± 20
5	800	47.8 ± .2	12.06 ± 2	.102 ± 1	0.323 ± 6
6	900	49.1 ± .3	16.43 ± 2	.077 ± 1	0.351 ± 5
7	1000	45.6 ± .3	16.47 ± 3	.066 ± 1	0.347 ± 6
8	1050	33.7 ± .3	10.07 ± 2	.061 ± 1	0.346 ± 7
9	1100	30.9 ± .3	7.81 ± 2	.062 ± 1	0.355 ± 9
10	1150	34.8 ± .3	7.45 ± 2	.079 ± 2	0.340 ± 19
11	1200	45.4 ± .3	8.83 ± 2	.105 ± 1	0.359 ± 9
12	1500	71.0 ± .3	23.00 ± 4	.119 ± 1	0.343 ± 4
13	1650	151.3 ± .4	1.45 ± 1	.504 ± 3	0.354 ± .136

VS3-18C   0.1021g   J = .0003077

step	T	^{40}Ar$_{tot}$	^{39}Ar	^{36}Ar	t ± 1 σ
1	500	86.39 ± 5	35.58 ± 4	.210 ± 2	0.3797 ± 93
2	600	158.3 ± .1	218.5 ± .2	.068 ± 1	0.3515 ± 10
3	800	66.33 ± 4	80.59 ± .10	.053 ± 1	0.3495 ± 18
4	1400	26.53 ± 2	21.82 ± 3	.042 ± 1	0.3581 ± 69

anh SH2   0.015g

step	T	^{40}Ar$_{tot}$	^{36}Ar
1	200	27.25 ± .41	.0909 ± 72
2	250	17.58 ± .39	.0614 ± 36
3	300	33.92 ± .33	.1029 ± 49
4	400	36.60 ± .30	.1291 ± 48
5	600	22.50 ± .20	.0638 ± 20
6	700	38.94 + .51	.1156 ± 15
7	1300	186.40 ± .41	.4296 ± 38

VU 1537-N   0.047g   J = .000478

step	T	$^{40}Ar_{tot}$	^{39}Ar	^{38}Ar	^{37}Ar	^{36}Ar	t ± 1 σ
1	500	297.1	8.62	.643	30.6	.946	2.01
		± .7	± 2	± 32	± 1.3	± 7	±.20
2	700	82.5	12.82	.405	84.8	.234	1.36
		± .7	± 2	± 28	± 4.2	± 3	± 6
3	800	74.5	32.56	.517	40.3	.155	0.85
		± .6	± 4	± 26	± 1.2	± 2	± 2
4	900	57.6	24.17	.357	9.1	.121	0.80
		± .5	± 4	± 24	± .9	± 3	± 3
5	1050	140.0	61.39	.916	9.8	.283	0.80
		± .4	± 7	± 46	± .5	± 3	± 1
6	1200	223.4	37.99	.643	23.0	.630	0.89
		± .3	± 5	± 26	± 1.0	± 5	± 3
7	1600	551.0	12.92	.548	87.2	1.757	2.60
		± .5	± 2	± 27	± 1.8	± 9	±.18

VU 1537-L   0.049g   J = .000478

step	T	$^{40}Ar_{tot}$	^{39}Ar	^{38}Ar	^{37}Ar	^{36}Ar	t ± 1 σ
1	500	765.0	3.43	.457	7.1	2.497	6.93
		± 1.1	± 1	± 22	± 1.1	± 11	±.80
2	700	136.8	83.31	1.241	136.3	.195	0.93
		± .2	± .16	± 37	± 2.7	± 3	± 1
3	800	89.0	69.82	1.210	27.7	.094	0.78
		± .3	± 8	± 30	± 1.4	± 3	± 1
4	900	84.1	33.19	.468	10.2	.174	0.87
		± .4	± 5	± 14	± 1.4	± 3	± 2
5	1050	99.4	15.12	.285	8.7	.285	0.90
		± .7	± 3	± 79	± 2.3	± 4	± 9
6	1200	79.7	9.61	.185	10.2	.222	1.33
		± .4	± 1	± 4	± 2.0	± 3	± 8
7	1600	1316.2	34.54	1.248	60.2	4.206	1.95
		± .7	± 4	± 13	± 1.8	± 18	±.13

Erebus   0.502 g   J = .000101

step	T	$^{40}Ar_{tot}$	^{39}Ar	^{38}Ar	^{37}Ar	^{36}Ar	t ± 1 σ
1	450	236.52	0.043	.173	.024	.874	22.15
		± .41	± 1	± 9	± 1	± 16	±4.27
2	600	54.10	0.264	.056	.082	.171	2.52
		± 5	± 1	± 1	± 1	± 1	±.21
3	750	42.31	1.331	.098	.446	.123	0.79
		± 5	± 2	± 1	± 3	± 1	± 2
4	850	67.92	1.806	.092	.713	.220	0.29
		± 8	± 3	± 1	± 3	± 1	± 4
5	950	148.00	1.380	.155	.489	.480	0.80
		± 9	± 3	± 1	± 3	± 2	± 8
6	1050	130.72	1.912	.152	.714	.418	0.67
		± 8	± 4	± 1	± 3	± 2	± 5
7	1150	79.85	3.229	.146	1.251	.240	0.50
		± .16	± 5	± 1	± 5	± 1	± 2
8	1250	39.70	4.482	.124	1.755	.112	0.27
		± .12	± 4	± 1	± 8	± 1	± 1
9	1600	46.45	4.094	.105	1.694	.150	0.10
		± 3	± 5	± 1	± 6	± 1	± 1

AL 42 a)

pl/g / 100°K

N-2 b)

pl/g / 100°K

● 40Ar
○ 39Ar

● 40Ar
○ 39Ar/10

AL 42 c)

$\frac{^{36}Ar}{^{40}Ar}$

Air

.003

.002

.001

N-2 d)

$\frac{^{36}Ar}{^{40}Ar}$
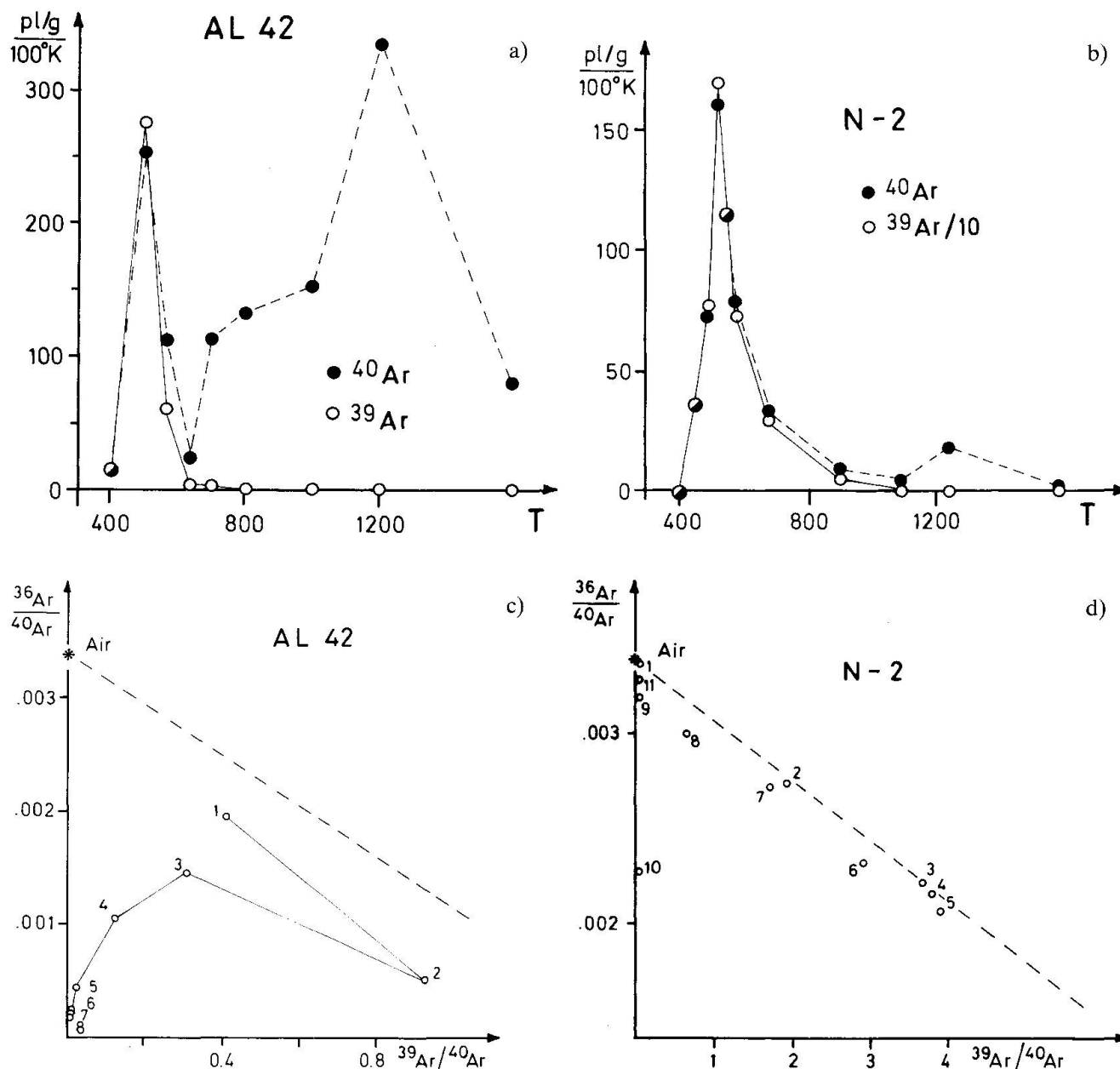
Air

.003

.002

Fig. 3 Behaviour of Ar isotopes in HEX-bearing leucites. (a) Differential release vs temperature for AL 42; (b) differential release vs. temperature for N-2. While ^{39}Ar (open circles) is released in a single temperature interval, ^{40}Ar has two humps ("camel"): a $^{40}Ar_K$ peak coincident with the ^{39}Ar peak, and a well-separated $^{40}Ar_{xs}$ peak at T > 1000°C. (c) Three-isotope ("isochron") plot for AL 42; (d) isochron for N-2. The trajectory of the individual steps deviate from the stratigraphic age (dashed reference line) due to addition of increasing proportions of $^{40}Ar_{xs}$, which plots at the origin.

cept, and pure ^{40}Ar is at the origin, so that excess-Ar-bearing steps plot below the isochron tying age and atmospheric Ar. The main source of uncertainties, as in all isochrons, is the subtraction of ^{36}Ar blank; for some of these leucites it is particularly critical, as the total ^{36}Ar is occasionally less than the average blank. Figure 3c shows one example where blank correction was less dramatic, AL-42. Especially remarkable is the 1200 °C step, whose measured $^{36}Ar/^{40}Ar$ ratio of (211.1 ±

1.4) × 10⁻⁶ becomes (158.2 ± 18.8) × 10⁻⁶ after blank subtraction, i.e. 20 times enriched with respect to atmospheric Ar.

This high-energy xs-Ar was called HEX by VILLA (1988). Another HEX-bearing sample, N-2 from VILLA (1991), is shown in figure 3d. The trajectory of its data points show the same characteristic trend: at T > 1000°C they plunge towards the origin, i.e. pure ^{40}Ar.

A leucite with a slightly saddle-shaped spec-

trum was reported by FUHRMANN and LIPPOLT (1986) who however did not elaborate on the excess nor on the small leucite-sanidine age disequilibrium.

3.2. Ar_{XS} IN SANIDINES

Unlike leucites, sanidines containing excess Ar display symmetric saddle spectra and their differential release plots do not show a clear-cut camel pattern. Some progress towards understanding Ar_{xs} as a geochemical tracer in sanidines has been made on samples from the Mt. Vulture Volcanic Complex. It is the easternmost center of the RVP; its products range from foiditic to phonolitic composition and have a number of geochemical peculiarities (DE FINO et al., 1986): their K_2O/Na_2O ratios are similar to those of the so-called "low-K series" (APPLETON, 1972) but their silica undersaturation and LILE enrichment are close to those of the "high-K series". In addition, S and Cl concentrations are high (total up to 3.5%). DE FINO et al. (1986) attribute the former two characteristics to a provenance from an anomalous mantle source, and the latter possibly to contamination with water having leached the underlying Cretaceous and/or Miocene evaporites. The high S concentrations are reflected in the ubiquitous presence of hauyne as the main feldspathoid, far more abundant than leucite (which is the dominant feldspathoid in all other centres of the RVP).

Over a dozen samples representing most lithostratigraphical formations were dated with the $^{40}Ar/^{39}Ar$ method. Most results have been presented by VILLA (1985b, 1988) and will be published in full elsewhere (LA VOLPE et al., 1991). The whole volcano was built up very quickly, between 740 and 560 ka bp; in such a short interval, stratigraphic bracketing is a powerful tool. While some samples yielded plateaus over 80% or more of the gas release, samples from other rocks displayed peculiarities whose implications extend beyond geochronology. These samples all have saddle-shaped spectra. In all cases, interpreting the minima of the saddles as maximum eruption ages allows the samples to fit into the general chronostratigraphic framework established by the plateau ages.

Three sanidine separates were analyzed from rock VU 1813 (see also VILLA, 1988, Fig. 2c). That from the total rock, VU 1813-T, has a deep saddle (Fig. 4), whose minimum at 0.72 Ma is probably very close to the eruption age, which is bracketed by plateaus on under- and overlying sanidines: 0.73 Ma > t > 0.67 Ma (LA VOLPE et al., 1991). It should be noted that the two bracketing sanidines
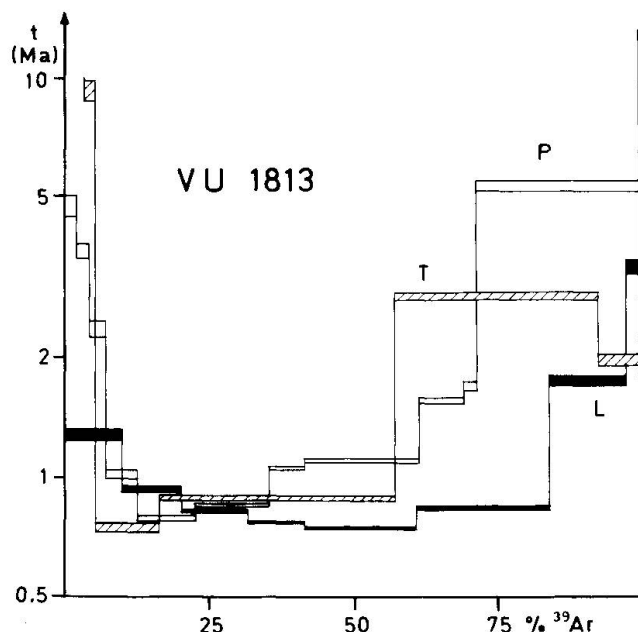

Fig. 4   Age spectra of sanidines VU 1813 (data in LA VOLPE et al., 1991). T, from total rock; P, five handpicked clear grains from pumices; L, leached T sanidines. Spectra T and P agree. $^{40}Ar_{xs}$ is removed by leaching; its introduction into the sanidine occurred thus after nucleation but before pumice formation.

displaying a plateau had been handpicked from pumices, which are known to better represent the original magma in a pyroclastite. There could have been the possibility that the irregular spectrum of VU 1813-T reflected the admixture of detritic feldspars contained in the groundmass, as had been observed in other settings by LO BELLO et al. (1987) and by LIPPOLT et al. (1986). To investigate this possibility, 5 sanidine grains, weighing a total of 10 mg, were handpicked from the remaining pumices. All 5 grains were clear, elongated crystals with regular faces, evidently young magmatic sanidines. The spectrum of the pumice sample, VU 1813-P, closely resembles that of -T (Fig. 4), as does the integrated $^{39}Ar/^{40}Ar$ age. This implies that all of the Ar_{xs} is a primary characteristic of this sample.

It is very important to re-emphasize that the five handpicked, magmatic sanidine grains from pumices (VU 1813-P) show the same spectrum as the total rock sanidines, VU 1813-T. This means that the presence of xenocrysts can be ruled out with absolute certainty (see also § 5), and that the discussion must look for other sources for Ar_{xs}, such as a fluid interacting with the magma prior to eruption. In order to try to constrain the depth at which incorporation of Ar_{xs} took place, one aliquot of VU 1813-T was leached in 20% HF for one hour and labelled VU 1813-L. The resulting

spectrum (Fig. 4) shows that a large part of the $^{40}Ar_{xs}$ was removed both at low and high temperatures. An explanation as to why leaching removed Ar_{xs} both at low *and* high temperature makes use of VILLA's (1988) two-site model: if an onionskin enriched in $^{40}Ar_{xs}$ is etched away, both tails of the saddle will undergo a reduction in their $^{40}Ar/^{39}Ar$ ratio. This means that the cores of the sanidines were less, if at all, affected by $^{40}Ar_{xs}$ which therefore was introduced at some intermediate stage of sanidine growth, later than nucleation but prior to pumice formation.

A sanidine from the Fara d'Olivo lava, VU 1537, was analyzed both untreated (aliquot N) and after leaching with diluted HF (aliquot L). The leaching lowered the Ca/K ratio by 30% but caused no loss of $^{40}Ar_{xs}$, as shown by the integrated Ar–Ar ages (1040 and 1120 ka, respectively); the stratigraphic age is known to be 730 ka. The spectra of VU 1537-N and -L are given by VILLA (1988, Fig. 2d). Thus, the obvious conclusion is that removal of Ca is decoupled from removal of Ar_{xs}.

It is important to note that in contrast to most Vulture samples $^{40}Ar_{xs}$ is absent from the coarse-grained leucite of the Cl, S-bearing hauynophyr VU 1523 (Fig. 1a). Since Cl and S are thought to derive from the shallow crustal evaporities (DE FINO et al., 1986), this implies that $^{40}Ar_{xs}$ was not carried by fluids circulating in the upper crust.

Excess Ar spectra in sanidines have been reported on a great number of samples by two groups (LIPPOLT et al., 1986; LO BELLO et al., 1987). In both papers, however, the origin of the saddle-shaped spectra was completely different from that of the RVP samples, being due to the admixture of Hercynian detrital feldspars to the Quaternary volcanic ones.

Finally, the existence of excess Ar does not necessarily imply that age excesses occur at high temperatures. The orthoclase megacryst from Erebus analyzed by VILLA (1988, Fig. 3) contains an Ar excess of 5×10^{-8} ml/g (or 0.1 ppb) contained both in fluid inclusions and in lattice positions but has the lowest step ages at high temperature. Note that these age gradients in no way have a geometrical counterpart, as the concentric zoning of the megacryst was disrupted by slicing (§ 2), but only reflect a variation in the binding energy of Ar isotopes. This topic will be addressed in the next paragraph. The Ca/K ratios are almost constant, between 0.71 and 0.83. Since there is no age increase at high temperature, and $^{40}Ar/^{36}Ar$ ratios progressively decrease, this sample contains no

HEX, despite the fact that $^{40}Ar_{xs}$ never reaches zero.

3.3. CORRELATIONS OF Ar_{xs} WITH Ca AND Cl

The question of the physical siting of Ar_{xs} has not been seriously addressed so far. The great advantage of the $^{40}Ar/^{39}Ar$ method is the fact that the neutron-produced isotopes (^{37}Ar from Ca, ^{38}Ar from Cl) can act as monitors for the elements they derive from. A correlation between Ar_{xs} and Cl has been proposed (CLAESSON and RODDICK, 1983, and references). A very suitable presentation to visualize this problem is that sketched in figure 5a, discussed in some detail by VILLA (1990). Briefly, the numerator, Ar_{rad} (defined as $^{40}Ar_{tot} - 295.5 \times ^{36}Ar_{atm}$) is composed of a truly radiogenic component, "kaliogenic" $^{40}Ar_K$, and of an "excess" component, $^{40}Ar_{xs}$. In this type of plot $^{40}Ar_K$ is represented by a point on the abscissa, A. Pure $^{40}Ar_{xs}$ plots at the origin; if it is accompanied by some Cl, but not by K, its representative point should lie on the ordinate axis (point X). If, additionally, one requires that this $^{40}Ar_{xs}$ has a fixed ratio to Cl, being a substituting atom in an anion vacancy*, then all experimental points must lie on the mixing line between X and A (line "model H" in Fig. 5a). VILLA (1990) noted that this was not the case for his microcline from Lhotse (Himalaya). He observed a positive correlation instead, but offered no explanation for this apparent positive correlation between K (cation) and Cl (anion). We shall return to this question at the end of this section.

Three examples of this plot are shown in figures 5b–d. In all cases, we know the eruption age, that is the kaliogenic Ar_K is uniquely determined. Figure 5b shows the Erebus orthoclase. As was the case for the GA-1 microcline (VILLA, 1990), points fail to follow model "H". The points instead follow a trajectory which starts near the origin (highest contribution of $^{40}Ar_{xs}$, i.e. highest step ages) then rises with a *positive* slope, decreases with a positive slope, and trends upwards, again with a positive slope. Point A corresponding to the eruption age (3.1 years) plots out of scale, at an x-value of 60133.3.

Figure 5c shows leucite N2. Once again, the points coarsely define an alignment with positive slope. The trajectory is downward, reflecting the fact that the Ar_{xs} increases with temperature (see Fig. 2a). Steps 1 and 2 are off-scale to the upper

---

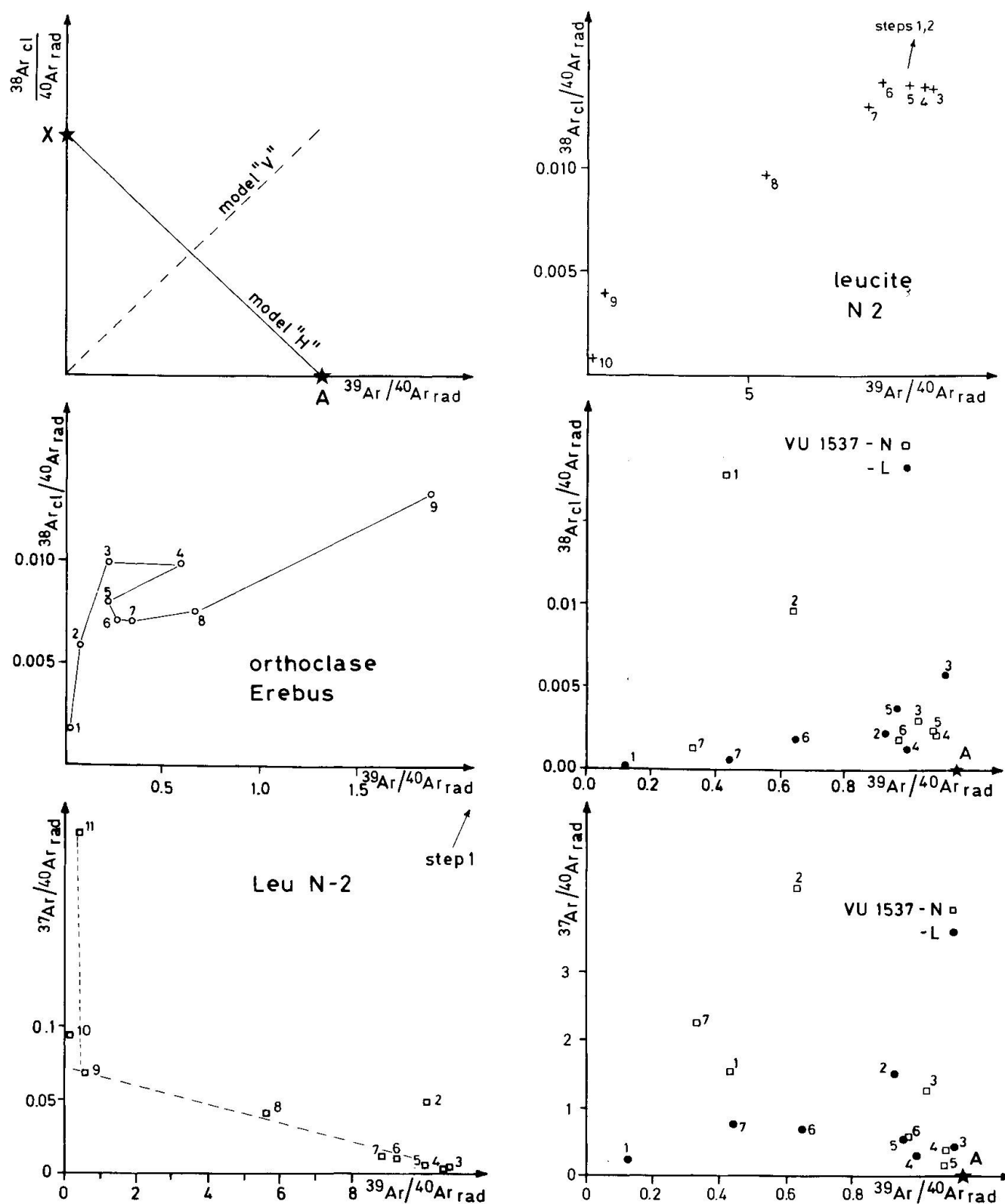* $^{38}Ar_{Cl}$ is produced by thermal neutrons, and thus does not recoil away from its "anion site".

Fig. 5 Three element correlation plot for Ar_{xs} bearing minerals. (a) Sketch of the expected ideal correlation of Ar_{xs} with Cl. If $^{40}Ar_{xs}$ is degassed by the same process as $^{38}Ar_{Cl}$, then we must observe a mixing between kaliogenic Ar (star A) and excess Ar (star X); in this plot, the binary mixing is the line labelled "model H". The other line, "model V", is predicted by the Ar_K and Ar_{Cl} transport mechanism described in § 3.3; addition of $^{40}Ar_{xs}$ in *variable* proportions to $^{40}Ar_K$ results in departures from the ideal straight line. The data points of (b) leucite N-2, (c) orthoclase Erebus, (d) sanidines VU 1537 all follow "model V" lines with addition of Ar_{xs}. (e) Ar_{xs}–Ar_{Ca} correlation plot for leucite N-2. One inverse correlation line is applicable to steps 3–9, but a different one is needed to fit HEXed steps 9–11. (f) Ar_{xs}–Ar_{Ca} correlation plot for sanidines VU 1537. The unleached fraction is scattered, the leached one suggests a "model V" line.

right. Especially noteworthy is the position of the HEXed steps, 9 to 11: they contain no chlorine-derived $^{38}Ar_{Cl}$. The so-called "anion sites" are degassed in steps 3–7 (full data in Tab. 1 of VILLA, 1991).

Finally, figure 5d illustrates the comparison between the two aliquots of VU 1537, the untreated one (N, open squares) and the HF leach residue (L, filled circles). The behaviour of the leached aliquot is rather similar to the unleached one: except for two points, all others are aligned along one and the same straight line.

The two odd-men-out are the 450 and 600 °C steps (numbered 1 and 2 in Fig. 5d) of VU 1537-N, which are much richer in chlorine than their leached counterparts (cfr. Tab. 1). They form a very crude alignment with the age end-member, A, and thus appear to suggest an excess end-member X with an ordinate value around 0.025. However, this "end-member" is only tenable for the low temperature steps, but the high-temperature points have absolutely no relation with it; moreover, point X does not represent a lattice component as the material represented by the 450 and 600°C steps was evidently completely removed by leaching. It is premature to speculate about the identity of this easily-leached material without detailed electron microscopy on the two mineral separates.

In summary, the K–Cl–Ar plot shows that despite the diversity of their spectral shapes all 4 samples have one common feature: $^{40}Ar_{xs}$ is clearly decoupled from $^{38}Ar_{Cl}$, i.e. anion sites. The fact that $^{38}Ar_{Cl}$ (produced with negligible recoil) correlates positively with $^{39}Ar_K$, despite the latter's recoil by ≈ 0.1 μm, may appear puzzling.

The existence of constant $^{40}Ar/^{39}Ar$ ratios in undisturbed samples implies that in these cases $^{40}Ar_K$ and $^{39}Ar_K$ atoms are transported by the *same* physical mechanism; this is traditionally interpreted to mean that they occupy the same crystal "sites". As the ^{39}Ar atoms recoil by about 100 cell widths, evidently their locations are not identical with the original sites of the ^{39}K targets; they might well be K vacancies (only 1–10 ppb K vacancies are typically required to accommodate all ^{39}Ar atoms of the present samples), but this is irrelevant, as the "siting" problem should really addressed both in terms of transport *paths* rather than pre-transport locations and by making use of a more realistic model of Ar mobility. What is usually called a "site" in stepwise heating should no longer be considered as a crystal-chemical lattice site from which Ar needs to be pried loose before it can freely move through an isotropic crystal. Rather, it can be argued that the factor controlling Ar mobility is the presence of defects

which need to be pushed all the way to the crystal surface. It follows that the two Ar atoms ($^{39}Ar_K$ and $^{38}Ar_{Cl}$), though they originate in crystal-chemically different environments, roughly correlate because they are pushing the same defects. Following this line of thought, the Ca/K ratio will be approximately constant if *only one* crystal species is present (this is indeed observed when pure, homogeneous minerals are analyzed); in order to bring about a variation, one must postulate that two distinct sublattices (e.g. Ab–Or) are being degassed, releasing ^{37}Ar and ^{39}Ar at different rates. Finally, as to the reason why $^{40}Ar_{xs}$ fails to correlate with any of the above, some indication may come from the experiment by VILLA and TRIGILA (1987), and the subsequent two-site model (VILLA, 1988). High-energy and low-energy defects ("H sites" and "L sites") are distributed throughout the crystal, and act as sinks for all Ar atoms which migrate through the lattice. From VILLA and TRIGILA's data, the abundance of the H sites is estimated to be < 1% of the L sites. In a natural mineral, most of the Ar_{xs} will thus be trapped in L sites, which are degassed at low energy; the mineral will lose most of its $Ar_{xs}(L)$ during its slow cooling (even volcanic minerals retain high temperatures for a few days); only a small part of it, along with most of the $Ar_{xs}(H)$, will be present in the laboratory separate. The neutron-produced isotopes $^{39}Ar_K$ and $^{38}Ar_{Cl}$, on the other hand, will partition > 99% into the L and < 1% into the H "sinks"; the latter will be consequently neglected on the correlation diagrams. A corollary of the two-site model is that the artificial Ar isotopes and Ar_{xs} will define a mixing line in figure 5a: the population of the H sites (mainly Ar_{xs}) will plot very close to the origin, that of the L sites (mainly reactor-produced Ar) will plot away from it; at increasing step temperature, the Ar(H)/Ar(L) ratios become progressively higher, shifting the data points down along the "model V" line. Leucite N2 appears to follow this trend (albeit not ideally).

Another plot which should reveal possible correlations is the $^{37}Ar/^{40}Ar_{rad}$ vs $^{39}Ar/^{40}Ar_{rad}$ correlation diagram shown in figures 5e–f. As in the preceding plot, it is possible to reveal a possible mixing between an age component, A, and a *calcium*-related excess Ar.

In the Erebus orthoclase, a correlation between Ar_{xs} and Ca is obviously absent, since K/Ca $\approx$ constant and $^{40}Ar_{xs}/K$ varies by 2 orders of magnitude. Another candidate siting for $^{40}Ar_{xs}$ are exsolved albite bodies (proposed, e.g., by ZEITLER and FITZGERALD, 1986). The diagnostic trend, similarly to figure 5a, is a line with *negative* slope tying A with some point X' on the ordinate axis.

Such a line seems suggested by the leucite N–2 (Fig. 5e), although the two HEX-rich steps, 9 and 10, define a different line from steps 3–8. It is possible that Ca-rich glass inclusions (cfr. § 5) contain some excess Ar, but at least two separate Ar_{xs} reservoirs are required to fit the present data.

Figure 5f shows sanidines VU 1537-N and -L. The pattern here is more complicated, especially that of the unleached aliquot (open squares). Points 1 and 2 stand apart, as was the case in figure 5d; the bulk of the gas is contained in steps 3–6, which can be tied either to point 7 or to point 2 to give a "model H" line. However, the leach residue is crucial for denying the validity of either such alignment. Indeed, the steps of aliquot L (filled circles) all have lower $^{37}Ar/^{40}Ar_{rad}$ ratios because a calcium-rich phase was preferentially leached away *without* affecting the Ar_{xs} concentration. The effect on the diagram is that in the "simplified" subcrystal assemblage of VU 1537-L ^{37}Ar and ^{39}Ar co-variate, as did ^{38}Ar and ^{39}Ar, independently of the Ar_{xs} release.

This does not mean that exsolved albite may never contain $^{40}Ar_{xs}$, it only proves that HEX siting is different in VU 1537.

4. Ar_{xs} in individual fluid inclusions

Six authigenic anhydrite grains (0.5 mm) from borehole SH2 in the Cesano geothermal field (Sabatini volcanic district, RVP) were analyzed with the $^{40}Ar/^{39}Ar$ laser microprobe. The fluid inclusions, from 2200 m depth, contain 0–10% NaCl and minor $CaSO_4$; their homogenization temperatures were uniform around 240–260 °C, slightly higher than the present-day in-hole temperature (BELKIN et al., 1988). The minerals are believed to have formed more recently than 100 ka bp. The radiogenic Ar produced in this short time in the virtually K-free grains is therefore negligible.

Anhydrite is almost transparent to the 1060 nm laser radiation. Whilst other, dark minerals are easily vaporized by the laser pulse and therefore release all their gas, the anhydrite was only slightly heated; on occasion the laser beam went straight through it and excavated small pits in the Al sample holder. However, a few laser shots were indeed absorbed by the saline fluid or by dark microimpurities and did release comparatively large amounts of Ar.

Although the permanent spectrometer background was only around 10^{-14} ml for masses 36 to 39, the amount of Ar released from a typical 20 mm diameter, 4 ng inclusions was frequently not much greater. Counting statistics creates a serious problem with count rates of 20–50 ions/

sec. Therefore, a different data treatment was required to extract semi-quantitative information without being overwhelmed by the very low signal/noise ratio.

Clearly, subtracting the background raises error bars inordinately. However, if three-isotope correlation diagrams for the raw data points are used, the correlations become apparent as straight tie-lines and the relevant end-members can be visually estimated. Figure 6a shows one such example, the uncorrected analogue of a $^{40}Ar/^{36}Ar$ vs $^{38}Ar/^{36}Ar$ plot. The crosses at the bottom right are representative of many machine background analyses and are collectively labelled B. As can be appreciated, the signal at masses 36 and 38 is not Ar (which would have been eliminated by suitable tube baking) but rather due to minor amounts of hydrocarbons and HCl (probably ppt chemical impurities in the steel used for the source). Asterisk A is air Ar. Also shown by several shots (circles) which only degassed atmospheric Ar adsorbed on the grain surface but decrepitated no fluid inclusions: they lie, as expected, on the A-B tieline. Points which are displaced to the upper right contain a mixture of A, B and a third component containing excess ^{40}Ar and ^{38}Ar produced by neutron irradiation of Cl. From the blank-corrected data we can constrain that end-member to have $^{40}Ar/^{36}Ar > 700$.

This high ratio is not derived from leaching the reservoir rocks (Mesozoic carbonates). The excess radiogenic Ar component derives from other sources: mantle or lower crust (see § 6). The ratio of Cl to air Ar in the fluid is similar to that found by KELLEY et al. (1986) and is compatible with a meteoric origin for the fluid itself.

Another 15 mg aliquot (consisting of a few 100–300 mm grains) of the same fluid-inclusion bearing anhydrite was analyzed, unirradiated, by stepwise heating in the RF oven in Pisa. The data are visualized in a differential release plot (Fig. 6b). Some gas, with a radiogenic $^{40}Ar/^{36}Ar$ ratio, appears to derive from decrepitation of fluid inclusions (T < 600 °C); surprisingly, a much higher amount of $^{40}Ar_{xs}$ is lattice-dissolved gas released only in the 1300 °C step. Captive minerals were not observed in SH2 (TECCE, pers. comm.). The temperature release pattern of "radiogenic ^{40}Ar" (i.e. $^{40}Ar_{tot} - 295.5 \times ^{36}Ar$) is very similar to that reported for quartz from Hemerdon Ball by KELLEY et al. (1986), who also suggested dissolved Ar as a possible explanation.

The geological information – though admittedly of lower quality than the rest of the present data, given the experimental difficulties and the minute gas amounts – is very important: it proves unambiguously that the fluids circulating in that
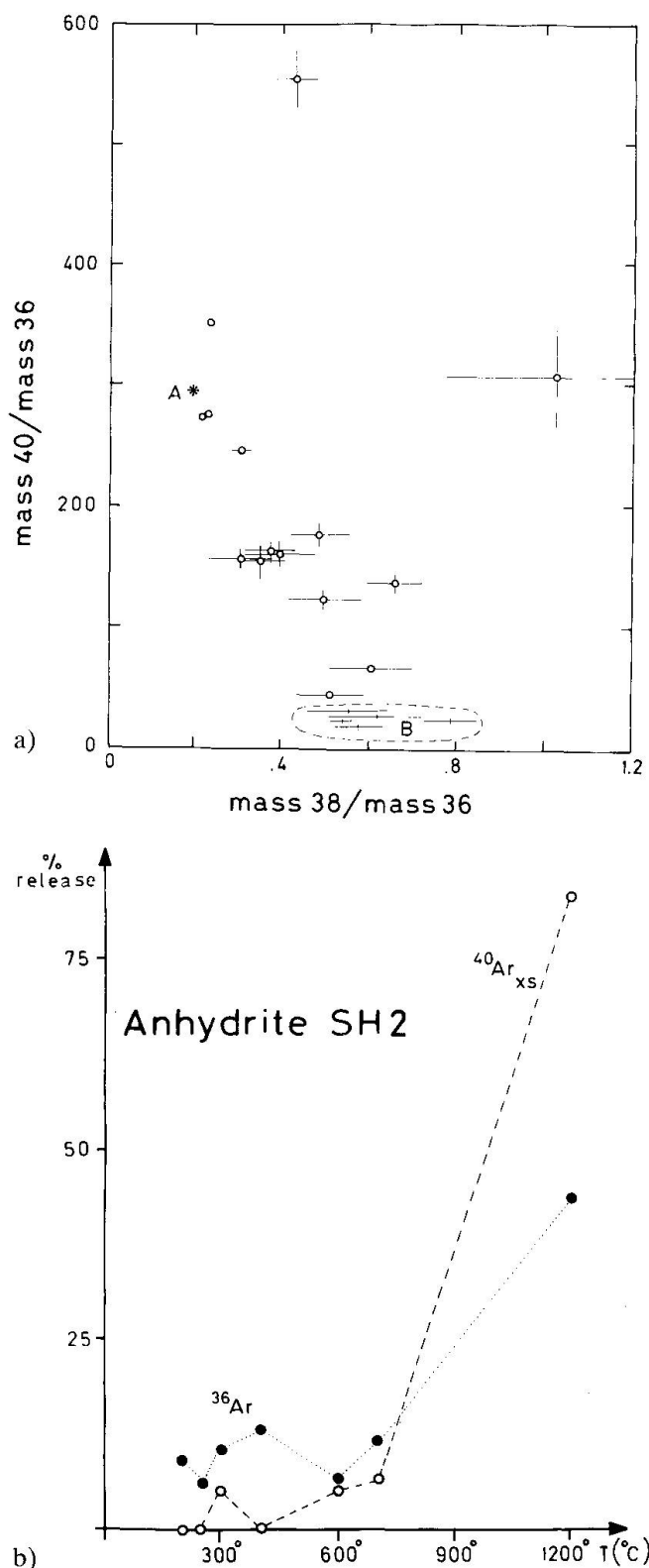
geothermal system were enriched in ^{40}Ar. This enrichment is not due to in-situ decay of K in anhydrite (K ≈ 100 ppm corresponds to a K/Ar age of the unirradiated sample of 1.8 Ma, compared with a stratigraphic age of ≈ 0.1 Ma), but purely to ^{40}Ar$_{xs}$.

5. The origin of ^{40}Ar$_{xs}$

The *primary* presence of ^{40}Ar not produced by in-situ decay of K in the volcanites has been demonstrated by analyzing magmatic minerals; the geochemistry of Ar can only be addressed by studying its behaviour and provenance in the magmatic minerals themselves, leaving aside secondary processes such as alteration.

The most usual cause of spectra whose step ages increase with temperature is the presence of a restite, a partly degassed xenocryst. This is surely not the case here, for several reasons.

(i) Restites are, by definition, leftovers of a preceding eruption, yet there is no (pre-) Carboniferous leucititic volcanism in Latium they could be left over from.

(ii) Restites and xenocrysts would show reaction rims with the host magma, while RVP leucites are typical equilibrium minerals.

(iii) Degassing of leucite is exceedingly easy in the laboratory (activation energies are around 20–30 kcal/mole: EVERNDEN et al., 1960; similar D_0 and E can be calculated from RADICATI et al., 1981) and it is unlikely that the old ages could have survived incorporation in a 900 °C magma for more than a few minutes.

(iv) Coarse-grained restites should be more retentive than fine-grained ones by a factor equal to the square of the radius ratio; this is the *opposite* trend as the data in § 3.1.

For this reason, the "extraneous" ^{40}Ar contained in the present samples is not "inherited" but indeed "excess" (all these terms follow LANPHERE and DALRYMPLE, 1976).

Secondary alteration of leucites is not a very likely origin for Ar$_{xs}$ either. Lavas and unwelded tuffs from the Alban Hills are mostly fresh, and samples were selected from a very wide and well-studied collection. The situation at Vulture is slightly worse, as many samples are fumarolized. Minerals of an altered rock, VU 1680, were described by VILLA (1988): while the sanidine spectrum resembled those of unaltered ones, the spectrum of the partly analcimized leucite showed significant differences in temperature release and general shape with spectra of near-stoichiometric leucites such as those shown in figure 2. The

Fig. 6 Ar isotopes in hydrothermal anhydrite SH2. (a) Raw data correlation plot for extremely gas-poor data points obtained by laser microprobe. A, atmospheric Ar. B, representative mass spectrometer background. Circles, gas released by single laser pulses. Only two shots degassed an inclusion (circles to the upper right), which contained ^{40}Ar$_{xs}$. (b) ^{40}Ar/^{36}Ar ratio vs temperature for oven-heated grains. Most of the ^{40}Ar$_{xs}$ is released in the 1300 °C step.

anomalous spectra are a characteristic of the fresh leucites. This reinforces the hypothesis that Ar_{xs} was acquired by a primary process during crystal growth and not due to secondary alteration.

Another possible candidate as carrier of Ar_{xs} are fluid inclusions. If fluid inclusions alone were responsible for the *high-temperature* Ar_{xs}, they should (i) contain a twentyfold enriched Ar, (ii) be decrepitated only above 800–900 °C. While isotopic enrichment of ^{40}Ar was indeed observed in fluid inclusions of the RVP (§ 4), its exact upper limit is poorly constrained; but, more importantly, the decrepitation of fluid inclusions is likely to take place between 300 and 600 °C, in a temperature range where the present leucites show small, if any, excesses. The only sample with a sizeable low-T excess that is probably due to fluid inclusions is the feldspar from Erebus; this sample happens to be the only one in this work without the high-T excess. Aqueous fluid inclusions were observed in kalsilite-bearing xenoliths similar to sample AL-44 (BELKIN et al., 1991). These authors interpret this record as evidence for a secondary recrystallization at shallow depth, possibly during the magma chamber residence of the Villa Senni Tuff magma. Last, but not least, fluid inclusions in leucites from lavas appear to be exceptional: one fluid inclusion was observed in an Alban Hills leucite by ROEDDER and COOMBS (1967, Fig. 4E) among a large number of "brownish glass inclusions"; however, it was the only one seen in a large survey and even its origin is still unexplained (ROEDDER, pers. comm, 1986). In leucite N-2, $^{40}Ar_{xs}$ and $^{37}Ar_{Ca}$ form a vague positive correlation, suggesting that the Ca-rich glass inclusions carry at least part of the excess. In fact, this only shifts the problem of enriching the leucites to that of enriching the residual liquid and efficiently preserving its Ar anomaly.

A direct contribution of fluid inclusions to the release of HEX is thus untenable, and the data require that the anomalous Ar is sited directly in the lattice. As shown by VILLA and TRIGILA (1987), HEX can be dissolved into the leucite lattice at 350 °C. This leaves open two possible explanations for the origin of $^{40}Ar_{xs}$:

– a comparatively low-temperature, shallow hydrothermal fluid, which gets its ^{40}Ar (with some ^4He) by leaching old crystalline basement rocks and interacts either with the magma (from which leucites grow, trapping the ambient enriched Ar) or with the formed crystals (at sufficient pT to allow dissolution into the leucite lattice);

– high-temperature magmatic gases, which relate to the mantle, the accepted source region of RVP magmas (HAWKESWORTH and VOLLMER, 1979) and which are enriched in ^{40}Ar and ^3He. An

attractive feature of this explanation is that it accounts for the correlation of Ar_{xs} with the primitivity of the volcanites: Ar_{xs} rises together with the magma if the latter ascends quickly (e.g. low differentiation index lavas) but will be lost if the magma rests and equilibrates at shallow levels (e.g. Villa Senni Tuff, Melfi hauynophir, kalsilite xenolith).

A third explanation, recycling of subducted marine sediments via low-degree partial melting, is often proposed as an origin for the K-rich RVP magmas. Without addressing the bulk of the geochemical argument, it should be noted that water-saturated sediments do not have Ar isotopic ratios exceeding 6,000 and thus cannot by the only source for Ar_{xs}.

The high Ar isotopic ratio alone does not discriminate among the first two possibilities, as both sources are characterized by very high $^{40}Ar/^{36}Ar$ ratios. The different He signature could decide the issue, but no combined argon-helium survey was performed on minerals from Italian volcanoes.

Note that involvement of mantle helium is established in virtually all present-day igneous activity centres (MAMYRIN and TOLSTIKHIN, 1984).

A purely crustal origin of the $^{40}Ar_{xs}$ in the RVP can be reasonably ruled out:

1. Samples with the highest crustal contamination (such as hauynophyr VU 1523) contain no HEX;

2. Sr–O isotopic correlations on Alban Hills lavas indicate "minor interaction with the continental crust" (FERRARA et al., 1985);

3. It is not known if the thick Neogenic carbonates and flysches underlying the volcanites (DURAZZO et al., 1983) are in turn underlain by Paleozoic basement rocks; if these exist at all, those deeper than 2.5–3 km depth lost practically all of their Ar (as observed by DEL MORO et al., 1982), so they hardly qualify as sources of a HEX component with a 20-fold enrichment.

A future effort will be trying to determine the exact limits of $^{40}Ar_{xs}$ distribution in other tectonic provinces and correlate its areal distribution with other anomalies, such as ^3He, LILE, etc., to better understand the meaning of mantle signatures.

6. Conclusions

The occurrence of saddle-shaped $^{40}Ar/^{39}Ar$ age spectra in sanidines of the RVP is primary in at least one case, where $^{40}Ar_{xs}$ was incorporated into already nucleated sanidines before pumice formation. In unaltered leucites, saddle spectra are

markedly unbalanced towards high temperatures and are a primary feature.

The high-energy excess component, HEX, is not related to the presence of restitic minerals. Comparison with artificial incorporation of ^{38}Ar in a manner resembling natural HEX (VILLA and TRIGILA) demonstrates that it is possible to dissolve HEX into leucite at temperatures much lower than magmatic ones.

The presence of ^{40}Ar$_{xs}$ is therefore proposed to be due to a deep circulation of an Ar-enriched fluid. This fluid could derive its Ar enrichment from interaction with old crust, but more probably incorporated mantle-derived magmatic gases; in this latter case, it should be possible to detect ^{3}He enrichments correlating with ^{40}Ar$_{xs}$.

References

APPLETON, J.D. (1972): Petrogenesis of potassium-rich lavas from the Roccamonfina volcano, Roman Region, Italy. J. Petrol., 13, 425-456.

BELKIN, H.E., CAVARRETTA, G., DE VIVO, B. and TECCE, F. (1988): Hydrothermal phlogopite and anhydrite from the SH2 well, Sabatini volcanic district, Latium, Italy: Fluid inclusions and mineral chemistry. Am. Mineralogist, 73, 775-797.

BELKIN, H.E., CAVARRETTA, G., DE VIVO, B. and TECCE, F. (1991): Aqueous inclusions in nodules from the Alban Hills volcano, Latium, Italy. Abstracts 11th ECROFI, Firenze, pp. 21-22.

BERNARDI, A., DE RITA, D., FUNICIELLO, R., INNOCENTI, F. and VILLA, I.M. (1982): Chronology and structural evolution of Alban Hills Volcanic Complex, Latium, Italy. Short Papers 5th Int. Conf. on Geochronology, Nikko, pp. 23-24.

BREWER, M.S. (1969): Excess radiogenic Ar in metamorphic micas from the Eastern Alps, Austria. Earth Planet. Sci. Lett., 6, 321-331.

CLAESSON, S. and RODDICK J.C. (1983): ^{40}Ar/^{39}Ar data on the age and metamorphism of the Ottfjællet dolerites, Særv nappe, Swedish Caledonides. Lithos, 16, 61-73.

DALRYMPLE, G.B. (1969): ^{40}Ar/^{36}Ar analyses of historic lava flows. Earth Planet. Sci. Lett., 6, 47-55.

DE FINO, M., LA VOLPE, L., PECCERILLO, A., PICCARRETA, G. and POLI, G. (1986): Petrogenesis of Monte Vulture volcano (Italy): inferences from mineral chemistry, major and trace element data. Contrib. Mineral. Petrol., 92, 135-145.

DEL MORO, A., PUXEDDU, M., RADICATI di BROZOLO, F. and VILLA, I.M. (1982): Rb–Sr and K–Ar ages on minerals at temperatures of 300–400 °C from deep wells in the Larderello geothermal field (Italy). Contrib. Mineral. Petrol., 81, 340-349.

DURAZZO, A., BERTINI, G., ROSSI, U. and MOTTANA, A. (1982): Syenitic intrusions intersected by Deep Drillings at Latera, Vulsini Mountains, Latium, Italy. N. Jb. Miner. Abh., 145, 239-255.

EVERNDEN, J.F., CURTIS, G.H., KISTLER, R.W. and OBRADOVICH, J. (1960): Argon diffusion in glauconite, microcline, sanidine, leucite and phlogopite. Am. J. Science, 258, 583-604.

FEDERICO, M. (1976): On a kalsilitoite from the Alban Hills, Italy. Per. Mineral., 45, 5-12.

FERRARA, G., LAURENZI, M.A., TAYLOR, H.P., TONARINI, S. and TURI, B. (1985): Oxygen and strontium isotope studies of K-rich volcanic rocks from the Alban Hills, Italy. Earth Planet. Sci. Lett., 75, 13-28.

FLISCH, M. (1982): Potassium-argon analysis. In: ODIN, G.S. (ed.), Numerical dating in stratigraphy, pp. 151-158. Wiley.

FOLAND, K.A. (1983): ^{40}Ar/^{39}Ar incremental heating plateaus for biotites with excess Ar. Isot. Geosci., 1, 3-21.

FUHRMANN, U. and LIPPOLT, H.J. (1986): Excess argon and dating of Quaternary Eifel volcanism: II. Phonolitic and foiditic rocks near Rieden, East Eifel/FRG. N. Jb. Geol. Paläont. Abh., 172, 1-19.

HAWKESWORTH, C.J. and VOLLMER, R. (1979): Crustal contamination versus enriched mantle: ^{143}Nd/^{144}Nd and ^{87}Sr/^{86}Sr evidence from the Italian volcanics. Contrib. Mineral. Petrol., 69, 151-165.

KELLEY, S., TURNER, G., BUTTERFIELD, A.W. and SHEPHERD, T.J. (1986): The source and significance of argon isotopes in fluid inclusions from areas of mineralization. Earth Planet. Sci. Lett., 79, 303-318.

LANPHERE, M.A. and DALRYMPLE, G.B. (1976): Identification of excess ^{40}Ar by the ^{40}Ar/^{39}Ar age spectrum technique. Earth Planet. Sci. Lett., 32, 141-148.

LA VOLPE, L., and 18 co-authors (1991): Carta vulcanologica del Monte Vulture. Serv. Geol. Ital., Roma.

LIPPOLT, H.J., FUHRMANN, U. and HRADETZKY, H. (1986): ^{40}Ar/^{39}Ar age determinations on sanidines of the Eifel volcanic field (Federal Republic of Germany): constraints on age and duration of a Middle Pleistocene cold period. Chem. Geol. (Isot. Geosci. Sect.), 59, 187-204.

LO BELLO, P., FERAUD, G., HALL, C.M., YORK, D., LAVINA, P. and BERNAT, M. (1987): ^{40}Ar/^{39}Ar step-heating and laser fusion dating of a quaternary pumice from Neschers, Massif Central, France: the defeat of xenocrystic contamination. Chem. Geol. (Isot. Geosci. Sect.), 66, 61-71.

MAMYRIN, B.A. and TOLSTIKHIN, I.N. (1984): Helium isotopes in nature. Elsevier.

RADICATI DI BROZOLO, F., HUNEKE, J.C., PAPANASTASSIOU, D.A. and WASSERBURG, G.J. (1981): ^{40}Ar/^{39}Ar and Rb/Sr age determinations on Quaternary volcanic rocks. Earth Planet. Sci. Lett., 53, 445-456.

ROEDDER, E. and COOMBS, D.S. (1967): Immiscibility in granitic melts indicated by fluid inclusions in ejected granitic blocks from Ascension Island. J. Petrol., 8, 417-451.

VILLA, I.M. (1985a): Ar excess and mantle provenance in leucites. Terra Cognita 5, 281.

VILLA, I.M. (1985b): Cronologia $^{40}Ar/^{39}Ar$ del complesso vulcanico del Monte Vulture. Rend. Soc. Ital. Miner. Petrol., 41, 146–147.

VILLA, I.M. (1987): SOS, a new zero-age standard, or: does $^{40}Ar_{xs}$ exist? Terra Cognita, 7, 252.

VILLA, I.M. (1988): Excess Ar in K-rich volcanites: the role of fluids. Rend. Soc. Ital. Miner. Petrol., 43, 95–104.

VILLA, I.M. (1990): Geochronology and excess Ar geochemistry of the Lhotse Nup leucogranite, Nepal Himalaya. J. Volc. Geoth. Res., 44, 89–103.

VILLA, I.M. (1991): Datability of Quaternary volcanites: an $^{40}Ar/^{39}Ar$ perspective on age conflict in lavas from the Alban Hills, Italy. Eur. J. Mineral., 3.

VILLA, I.M. and TRIGILA, R. (1987): Artificial $^{38}Ar_{xs}$ in doped leucite. Terra Cognita, 7, 330.

WASHINGTON, H.S. (1906): The Roman Comagmatic Region. Carnegie Inst., Washington, Spec. Publ. 57.

ZEITLER, P.K. and FITZGERALD, J.D. (1986): Saddle-shaped $^{40}Ar/^{39}Ar$ age spectra from young, micro-structurally complex potassium feldspars. Geoch. Cosm. Acta, 50, 1185–1199.